Australian Government
Department of Defence
Defence Science and Technology Group

Doppler Compensation for Airborne Non-Side-Looking Phased-Array Radar

Yunhan Dong

National Security and ISR Division
Defence Science and Technology Group

DST-Group-TN-1461

ABSTRACT

As a supplement to an earlier DSTO Technical Note, *Overview of STAP algorithms*, this Technical Note examines processing of phased array data collected from non-side-looking geometries. Space-time adaptive processing (STAP) algorithms developed for the radar operating in the side-looking mode cannot in general be directly applied to radar operating in non-side-looking modes, including the forward-looking mode. A simple Doppler compensation scheme is described, so that the Doppler frequency of mainlobe clutter is shifted to zero and becomes range invariant, like the clutter data collected from the side-looking geometry. After Doppler compensation, all STAP algorithms developed for the side-looking geometry can be applied. Also briefly discussed are some techniques for suppression of range-ambiguous clutter, including so-called 3D STAP and frequency diversity technology.

Published by

National Security and ISR Division
Defence Science and Technology Group
PO Box 1500
Edinburgh South Australia 5111 Australia

Telephone: 1300 333 362
Fax: (08) 7389 6567

AR-016-420
September 2015

APPROVED FOR PUBLIC RELEASE

Doppler Compensation for Airborne Non-Side-Looking Phased-Array Radar

Executive Summary

Australian Defence Force (ADF) has been equipped with the Wedgetail Airborne Early Warning and Control (AEW&C) system since 2009, providing an entirely new capability for surveillance that gathers essential and necessary information from air and surface surveillance areas.

One of key sensing elements of the Wedgetail AEW&C system is the airborne L-band phased array radar system. When its side arrays are operated in the side-looking geometry, the earth surface has a Doppler shift which is range invariant. For a homogeneous clutter environment, the collected data with respect to range, after some normalisation treatment, can be considered as independent and identically distributed (i.i.d.) samples, providing a means for estimating the covariance matrix of unknown interferences. The covariance matrix or the like is essential for the optimal detection of targets of interest. Numerous fully-adaptive and partially-adaptive space-time adaptive processing (STAP) algorithms have been developed for the processing of the phased-array data collected from this side-looking geometry.

When a phased array radar steers away from the side-looking direction, the Doppler shift of mainlobe clutter becomes range dependent, making range samples non-i.i.d. If a STAP algorithm developed for the side-looking geometry is directly applied to the data collected from non-side-looking geometries, detection loss occurs especially in the vicinity of the mainlobe clutter Doppler. In addition, there are also more false-alarms than desirable as the processor cannot sufficiently suppress the mainlobe clutter. Therefore, the STAP algorithms developed for the side-looking mode cannot in general be directly applied to non-side-looking geometries.

Fortunately, the range-dependent Doppler shift of mainlobe clutter is totally determined by the parameters of radar and platform, and independent of the clutter environment. Following previous publications in the literature, this Technical Note describes a simple Doppler compensation scheme. Under this scheme, data collected from a non-side-looking geometry first undergoes a Doppler compensation. After the compensation, the Doppler frequency of mainlobe clutter is shifted to zero and becomes range invariant, like the data collected from the side-looking geometry. All the STAP algorithms can then be applied. The detection improvement by this Doppler compensation scheme has been demonstrated using the data generated by DSTO's

GPARM (stands for Generic Phase Array Radar Modelling) radar system simulation software.

The suppression of range-ambiguous clutter is also addressed. Among a few techniques discussed, the simplest implementation is the beamforming in elevation in some cases. For radar looks at near range, depression angles of the mainlobe clutter and the range-ambiguous clutter can be very different. A beamforming in elevation, if available, can null the illumination of the range-ambiguous clutter to achieve clutter suppression. 3D STAP (azimuth, elevation and Doppler adaptive processing) can be considered, if measurements in elevation array elements are available and the computational cost affordable. The 3D STAP provides extra degrees of freedom (DoF), so the clutter coming from different elevation angles can be suppressed. The drawback of 3D STAP is the significant increase in the requirements of sample data and computational load.

The frequency diversity technology where different channels of an array are transmitting of different frequencies but on receive the whole array receives and processes the entire transmitted frequencies has the potential to provide suppression of range ambiguous clutter. A frequency diverse waveform generates a periodic range dependent beam pattern which enables range ambiguous clutter to be managed by careful selection of the range ambiguity interval relative to the underlying periodicity of the range dependent beam pattern generated by the frequency diverse waveform. Detailed architectures, characteristics and techniques of the frequency diverse array radar will be studied, investigated and analysed in a separate report.

Author

Yunhan Dong
National Security and ISR Division

Dr Yunhan Dong received his Bachelor and Master degrees in 1980s in China and PhD in 1995 at UNSW, Australia, all in electrical engineering. He then worked at UNSW from 1995 to 2000, and Optus Telecommunications Inc from 2000 to 2002. He joined DSTO as a Senior Research Scientist in 2002. His research interests are primarily in radar signal and image processing and clutter analysis. Dr Dong was a recipient of both the Postdoctoral Research Fellowships and Research Fellowships from the Australian Research Council.

This page is intentionally blank

Contents

Acronyms

ADF	Australian Defence Force
AEW	airborne early warning
CNR	signal-to-noise ratio
CPI	coherent processing interval
DoF	degrees of freedom
FDA	frequency diverse array
GMTI	ground moving target indication
GPARM	generic phased array radar model
i.i.d.	independent and identically distributed
PRF	pulse repetition frequency
PRI	pulse repetition interval
RCS	radar cross-section
SINR IF	signal-to-interference-and-noise ratio improvement factor
SLAR	side-looking airborne radar

1. Introduction

Airborne radar systems generally seek to be able to detect targets with a low range rate either to facilitate the detection of "beaming" aircraft or for the detection of surface moving targets (i.e. ground moving target indication (GMTI)). For airborne phased array radar space-time adaptive processing (STAP) optimally improves the detection performance against slow moving targets. The detection of slow moving targets must be achieved against a background of radar returns from the Earth's surface (surface clutter) which has an apparent Doppler shift due to the interaction of the finite beam width from the antenna on a moving aircraft. The scientific literature has identified a number of adaptive signal processing techniques to produce filters that will minimise the impact of clutter on the radar system, and many of these techniques require training data from independent and identically distributed (i.i.d.) samples to provide the statistical information to optimise the suppression of clutter whilst minimising the impact on potential targets. The radar literature (Klemm 2002; 2004; Guerci 2003; 2010; Ward 1994; Melvin 2004; Himed *et al.* 2013) primarily considers side-looking radar systems because for a radar system that is looking perpendicular to the velocity vector the dominant clutter return produced by the antenna mainlobe intercepting the Earth's surface has a Doppler spectrum which is range invariant, which is necessary to meet the requirement for "identically distributed".

The operational utility of an airborne radar system is significantly enhanced if the constraints on the look direction of the radar system necessary to obtain optimal performance are minimised; in this case the ability to obtain optimal performance when the radar is scanned well away from the side-looking direction. Some of the literature (Wang *et al.* 1997; Kreyenkamp and Klemm 2001; Lapierre *et al.* 2009) has examined non-side-looking geometries. In this report we further develop these techniques to extend the performance of algorithms developed for the side-looking case to a wider angular coverage.

All fully-adaptive and partially-adaptive STAP algorithms inclusively need to estimate the covariance matrix of unknown interferences or the like to implement the adaptive processing. Ideally the estimation requires range samples to be i.i.d. Unfortunately, the data collected from a non-side-looking geometry are Doppler range-dependent and hence not i.i.d. even if the clutter environment itself is homogenous. Use of non-i.i.d. samples for estimating the covariance matrix or the like violates the estimation requirement.

The fundamental difference between the clutter data collected from non-side-looking and side-looking geometries lies in that the former in general exhibits range dependent Doppler, violating the i.i.d. assumption that is implicitly applied to techniques and algorithms developed for the side-looking geometry. Fortunately, the Doppler response of the Earth surface clutter is determined by the radar and platform parameters making it possible to compensate the Doppler from range bin to range bin in such a way that the Doppler appears to be statistically identical for all range samples, like the Doppler range invariant data collected from the side-looking geometry. Once the Doppler compensation is done, the data can be treated as if they were collected from the side-looking geometry,

and hence all the techniques and algorithms developed for that geometry can be applied directly.

It is worth noting that the role of GMTI may not be compromised for the non-side-looking mode[1]. Although the mainlobe clutter has a nonzero Doppler shift for radar looking into a non-side-looking direction, it is only the relative velocity of target to the ground matters. The relative motion between the radar's main beam and the ground only results in a Doppler shift but does not change the Doppler difference between the target and the clutter, assuming the target's radial velocity relative to the ground to remain the same.

This Technical Note is a supplement of an earlier Technical Note (Dong 2011), to include the processing of non-side-looking data for AEW radar. Section 2 describes the range-dependent Doppler of non-side-looking data and its compensation. Section 3 presents a numerical example showing the effectiveness of the Doppler compensation scheme proposed in this note. In addition, range-ambiguous cases are discussed in Section 4. Also discussed in Section 5 are techniques of 3D STAP and the frequency diversity technology aiming at suppression/mitigation of range-ambiguous clutter to improve the performance of GMTI. Section 6 concludes the note.

2. Range-Dependent Doppler and Its Compensation

Figure 1 depicts geometries of forward-looking and side-looking airborne arrays. The ground is approximated to a horizontal plane and the platform flies horizontally in the x direction with a velocity of v_a. The forward-looking array is the array whose boresight is in the x direction and the side-looking array is the one with its boresight in the y direction. Owing to the relative movement between the array and a stationary scatterer located at P on the ground, the Doppler frequency of the scatterer measured by the radar is (Klemm 2002, Chapter 1; Ward 1994),

$$f_a = \frac{2v_a}{\lambda}\cos\theta\cos(\phi - \phi_a) \qquad (1)$$

where λ is the wavelength of carrier frequency, θ is the depression angle (under the assumption, it is also the grazing angle), ϕ is the azimuth angle and ϕ_a is the aircraft's drifting (crabbing) angle, i.e., the actual flying direction is away from the x-direction by ϕ_a normally due to the atmospheric wind effects.

[1] This is especially true for radar operated in the range-unambiguous low PRF mode.

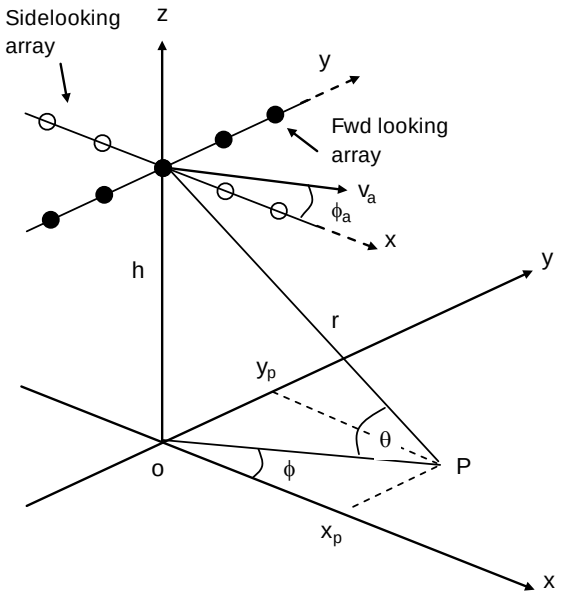

Figure 1: Geometry of forward-looking and side-looking airborne arrays.

The depression angle is a function of the ratio of platform height h to range r, resulting in,

$$f_a = f_{a\max}\sqrt{1-\left(\frac{h}{r}\right)^2}\cos(\phi-\phi_a) \qquad (2)$$

where $f_{a\max} = 2v_a/\lambda$ is the maximum Doppler frequency the ground clutter can have. It can be seen that the Doppler frequency is dependent on the ratio of h/r whenever $\cos(\phi-\phi_a)\neq 0$ (i.e. non side-looking situations).

The normalised surface clutter Doppler (isodops) of the whole surface is shown in Figure 2 where the platform flies horizontally in the x direction without any crabbing angle ($\phi_a = 0$), coordinates of (x, y) are also normalised by the platform height h. The maximum positive Doppler and negative Doppler are reached at $(\infty,0)$ and $(-\infty,0)$, respectively, whereas zero Doppler is kept along the whole $\pm y$ directions (the side-looking geometry).

Shown in Figure 3 is the range-dependency of normalised Doppler for mainlobe clutter when the radar steers towards three non-side-looking directions, namely, 0^o from nose (forward-looking), 30^o from nose and 60^o from nose, respectively. It can be seen that the range-dependent Doppler varies significantly at near ranges (low r/h ratios). At far ranges (e.g. $r/h > 10$), the Doppler of mainlobe clutter becomes approximately range invariant although the magnitude of the Doppler is still dependent on the look direction.

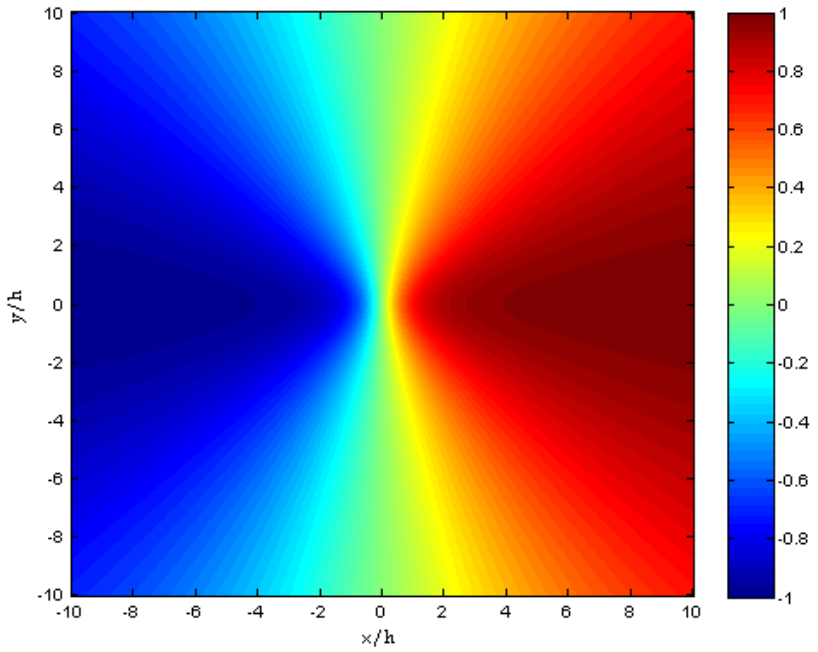

Figure 2: Normalised surface clutter Doppler (the isodops) when the platform flies horizontally in the x-direction.

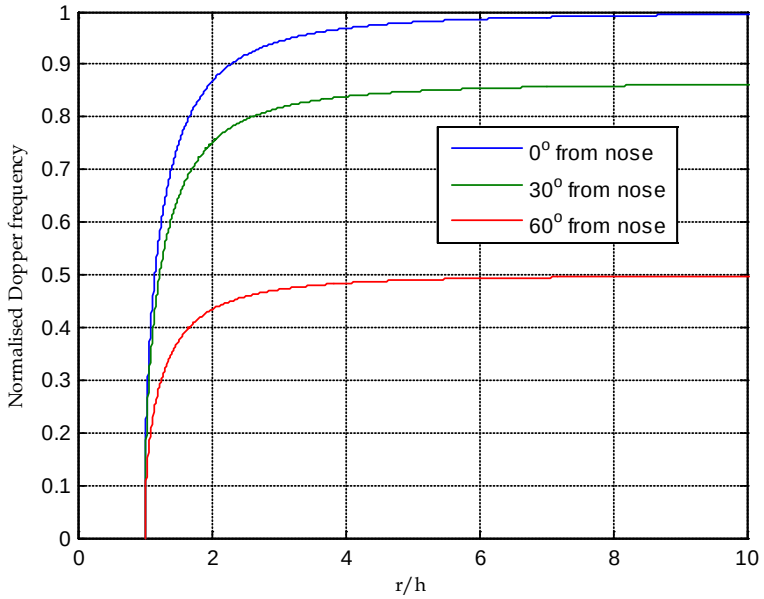

Figure 3: Range dependency of the normalised Doppler frequency of mainlobe clutter (0^o from nose is the case of radar looking in the flight direction).

Shown in Figure 4 are two half surface rings, corresponding to two different ranges, for radar operated in the forward-looking geometry. Clutter signal received by antenna element n, pulse m at range r is an integral of the echoes from the constant range ring (returns from ambiguous range are not included here and will be discussed later), given by,

$$\chi_r(n,m) = \sum_{\phi_k=-\pi/2}^{\phi_k=\pi/2} \xi(\theta,\phi_k) e^{j2\pi n f_s} e^{j2\pi m f_a T_r} \quad \text{for} \quad n = 0,1,\cdots,N-1 \text{ and } m = 0,1,\cdots,M-1 \qquad (3)$$

where $\xi(\theta,\phi_k)$ is the backscattered field from an clutter patch area of $\Delta A_k = r\cos\theta\,\Delta r\,\Delta\phi_k$ at (θ,ϕ_k) (range r and height h determine the depression angle θ), Δr is the radar's range resolution; $T_r = 1/f_{PRF}$ is the pulse repetition interval (PRI) and f_{PRF} is the pulse repetition frequency (PRF); f_s and f_a are the spatial and temporal frequencies, respectively. The reason for the integration of a half ring only is that the backlobes of the antenna are assumed to be small enough to be ignored. Quantities in (3) are further discussed in the following.

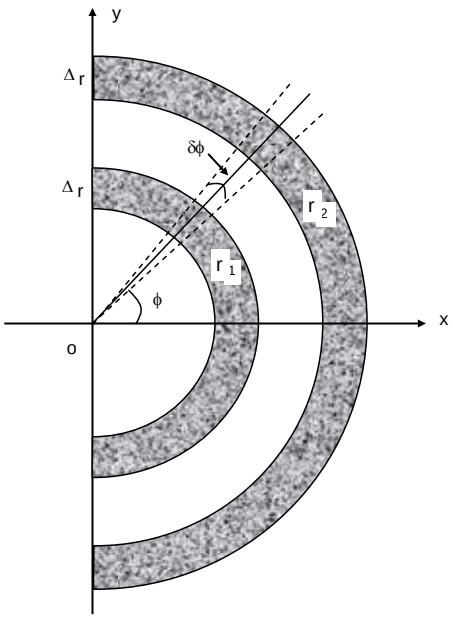

Figure 4: Clutter signal collected by an antenna element for a pulse is an integral of scattering fields from all scatterers in a half ring (two rings corresponding to two different ranges are shown).

The backscattered field may be written as $\xi(\theta,\phi_k) = |\xi(\theta,\phi_k)|e^{j\varphi_k}$ where φ_k is the initial phase of the clutter patch relative to the reference. Since phase centres of scatterers are random, the initial phase can be assumed to be random, if clutter patches are mutually uncorrelated. The amplitude of backscattered field may be determined from the radar equation should the backscattering coefficient be known, as (Ward 1994),

$$E\left\{\left|\xi(\theta,\phi)\right|^2\right\}=\frac{P_t T_p G(\theta,\phi_k) g(\theta,\phi_k)\lambda^2\sigma_0(\theta,\phi_k)\Delta A_k}{(4\pi)^3 L_s r^4} \quad (4)$$

where P_t is the transmitted power, T_p is the pulse width; G and g are the full array transmit gain and the element receive gain, respectively; σ_0 is the backscattering coefficient and L_s denotes the total loss for the radar system. The single-element single-pulse clutter-to-noise ratio (CNR) is,

$$CNR = E\left\{|\xi|^2\right\}/\sigma^2 \quad (5)$$

where σ^2 is the variance of thermal noise.

For an array operated in the forward-looking mode and flying in the x-direction with no crab angle ($\phi_a = 0$), the spatial and temporal frequencies are, respectively (Klemm 2002; Ward 1994),

$$f_a = \frac{2v_a}{\lambda}\cos\theta\cos\phi_k \quad (6)$$

$$f_s = \frac{d}{\lambda}\cos(\theta-\theta_s)\sin\phi_k \quad (7)$$

where θ_s is the array tilted angle. Often radar is pointed to the area of interest for detection, which means its mainlobe is pointed to the area of interest, so that $\cos(\theta-\theta_s)\approx 1$.

As indicated by (6), the Doppler frequency of mainlobe clutter ($\cos\phi_k = 1$), when the radar system is operated in the forward-looking mode, is,

$$f_{a0} = \frac{2v_a}{\lambda}\cos\theta = \frac{2v_a}{\lambda}\sqrt{1-\left(\frac{h}{r}\right)^2} \quad (8)$$

Equation (8) clearly shows the range-dependency of the mainlobe clutter for radar operated in the forward-looking mode. While the mainlobe clutter shall be dominant in the received clutter signal, contributions of clutter returns from other azimuths should not be ignored, and their relative strengths are largely determined by transmit and receive gains as well as the backscattering coefficient as indicated by (4).

For the purpose of demonstration, Table 1 lists parameters of a simple airborne linear phased array used in the simulation. According to parameters, the transmit beam pattern

(the whole array beam pattern) and the element receive beam pattern are shown in Figure 5 and Figure 6, respectively.

Table 1: Parameters used in the simulation

Parameter	**Value**
Platform height, h	5000 m
Platform velocity, v_a	150 m/s
Pulse repetition frequency, f_{PRF}	3200 Hz
Carrier waveform length, λ_0	0.25 m
Bandwidth of LFM	5 MHz
Sampling rate	10 MHz
Number of array elements, N	25
Number of pulses in a CPI, M	31
Antenna element beam pattern in azimuth	$\cos\phi$

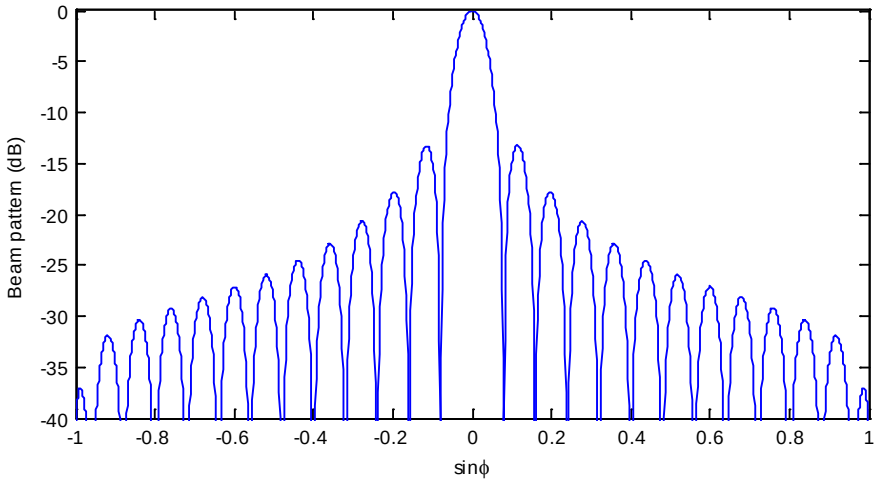

Figure 5: One-way full array azimuth beam pattern (transmit) used in the simulation.

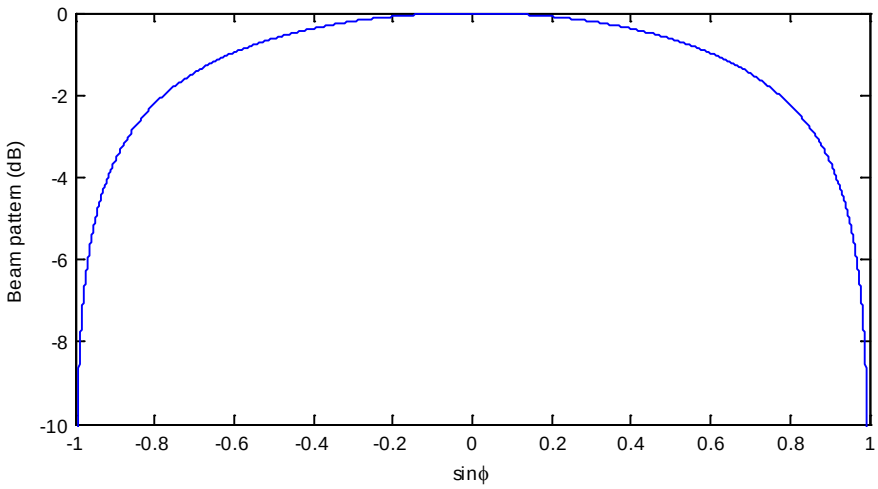

Figure 6: One-way element azimuth beam pattern (receive) used in the simulation.

Using the parameters given in Table 1, clutter received by receive elements are simulated using (3). In the simulation, the dependency of clutter intensity upon range, as shown in (4), is normalised. The backscattered field is determined assuming the backscattering coefficient σ_0 to be a constant and the associated initial phase to be random but uniformly distributed in $[0, 2\pi]$. Therefore, the clutter intensity received from ring r_1 and ring r_2 shall be statistically identical with Doppler frequencies being different and dependent on range as shown in (6). The single-element single-pulse CNR is set to 30 dB. The simulated data for each range bin are stored in a two-dimensional $N \times M$ matrix, where N and M denote the number of array elements and the number of pulses in a coherent processing interval (CPI), respectively.

Figure 7 shows the pulse-based M beamformed clutter spatial spectra (i.e., each column of the $N \times M$ matrix is beamformed) using the simulated clutter data for a radar operating in the forward-looking mode with $r/h = 2.0$ (a near range case). The channel-based N Doppler spectra (i.e., each row of $N \times M$ matrix is Fourier transformed) are shown in Figure 8. For comparison, the spatial spectra and Doppler spectra for $r/h = 20$ (a far range case) are shown in Figure 9 and Figure 10, respectively. It can be seen that the spatial spectra are statistically identical for the near range and far range cases. The only difference between the two cases is their Doppler spectra that peak at 1039.2 Hz for $r/h = 2.0$ and 1198.5 Hz for $r/h = 20$, respectively, according to (8). It is worth noting that in the simulation, the backscattering coefficient σ_0 is assumed to be a constant and the associated phase to be random with a uniform distribution in $[0, 2\pi]$.

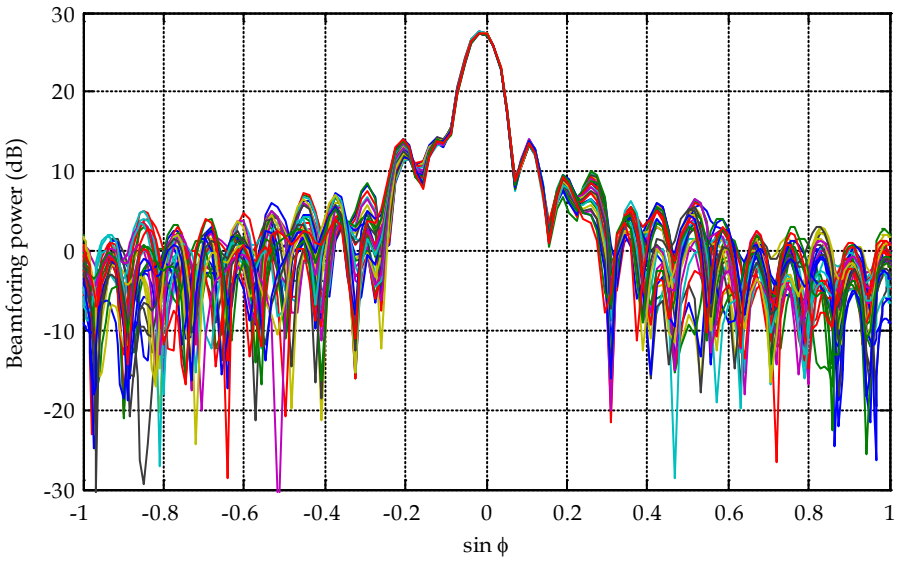

Figure 7: Pulse-based M spatial clutter spectra beamformed from the simulated clutter data for a radar operating in the forward-looking mode with $r/h = 2.0$.

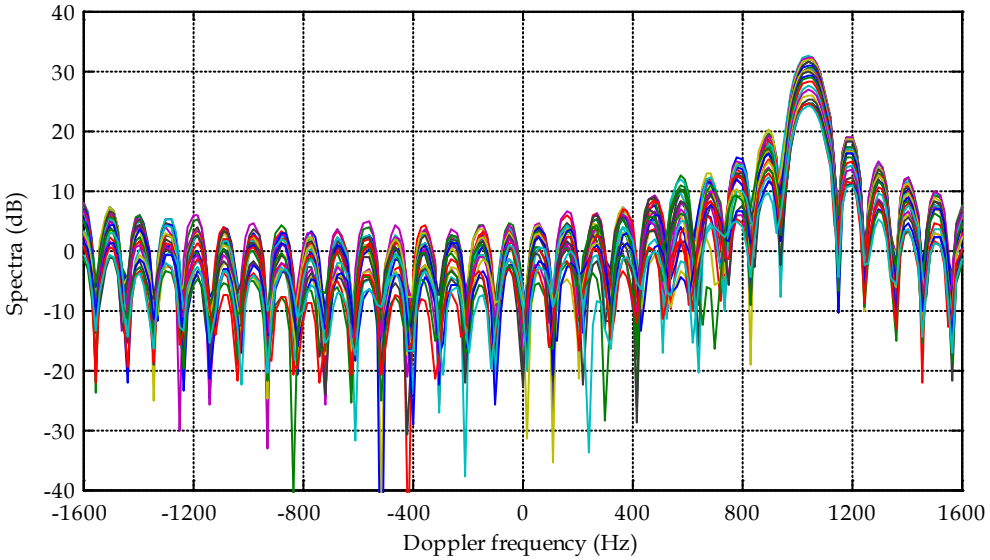

Figure 8: Channel-based N Doppler spectra of the simulated clutter data for a radar operating in the forward-looking mode with $r/h = 2.0$ *(The Doppler frequency peaked at 1039.2 Hz).*

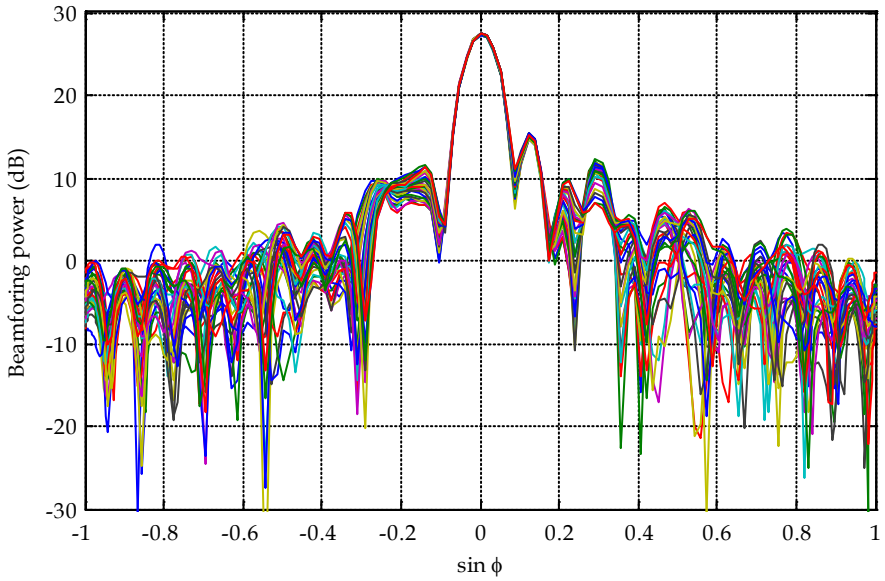

Figure 9: Pulse-based M spatial clutter spectra beamformed from the simulated clutter data for a radar operating in the forward-looking mode with $r/h = 20$.

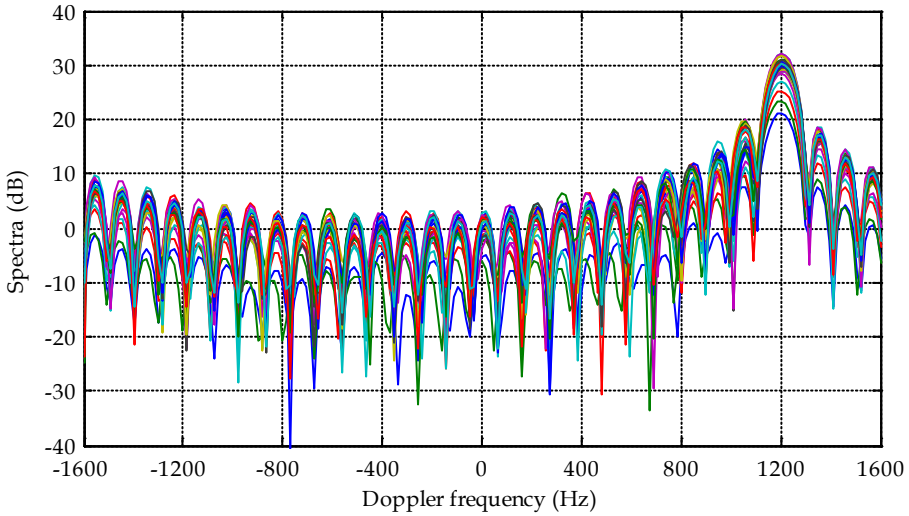

Figure 10: Channel-based N Doppler spectra of the simulated clutter data for a radar operating the in forward-looking mode with $r/h = 20$ *(the Doppler frequency peaked at 1198.5 Hz).*

If the Doppler spectra shown in Figure 8 is circularly shifted by a proper amount, so that their peak have the same Doppler frequency as that of the Doppler spectra shown in Figure 10, then the former data can be considered as if the data were collected at the latter's r/h.

Mathematically, if $F(f)$ is the Fourier transform of $f(t)$, then $F(f-\Delta f)$ corresponds to the Fourier transform of $f(t)e^{j2\pi\Delta f t}$. Accordingly, let $\chi_r(n,m)$ and $\chi_{r_0}(n,m)$ denote clutter data collected at ranges r and r_0, respectively, for $n = 0,\cdots,N-1$ and $m = 0,\cdots,M-1$, and let

$$\Delta f = \frac{2v_a}{\lambda}\left[\sqrt{1-(h/r_0)^2} - \sqrt{1-(h/r)^2}\right] \qquad (9)$$

then the operation of

$$\chi_r'(n,m) = \chi_r(n,m)e^{j2\pi\Delta f\, mT_r} \quad \text{for} \quad n = 0,\cdots,N-1 \text{ and } m = 0,\cdots,M-1 \qquad (10)$$

compensates the Doppler frequency of $\chi_r(n,m)$ as if $\chi_r'(n,m)$ were collected at range r_0. It is noted that the operation of (10) does not alter spatial spectra of the data. Equation (10) may be written as a compact vector form of,

$$\boldsymbol{\chi}_r' = \boldsymbol{\chi}_r \circ \mathbf{q}_r \qquad (11)$$

where snapshot $\boldsymbol{\chi}_r$ is an $NM \times 1$ vector and formed by stacking the data $\chi_r(n,m)$, $n = 0,\cdots,N-1$, and $M = 0,\cdots,M-1$; the symbol $\circ$ denotes element-by-element multiplication, and $\mathbf{q}_r$ the corresponding Doppler compensation vector as,

$$\mathbf{q}_r = \mathbf{s}_c \otimes \mathbf{1}_{N\times 1} \tag{12}$$

where $\otimes$ denotes Kronecker product and,

$$\mathbf{s}_c = \left[1 \quad \exp(j2\pi\,\Delta f\, T_r) \quad \cdots \quad \exp(j2\pi(M-1)\Delta f\, T_r)\right]^T \tag{13}$$

In application, one may designate $r_0 = h$, the Doppler frequency to be compensated becomes,

$$\Delta f = -\frac{2v_a}{\lambda}\sqrt{1-(h/r)^2} \tag{14}$$

The advantage of using (14) for compensating Doppler for range-dependent forward-looking clutter is that the Doppler of the mainlobe clutter becomes zero after the compensation, which is the same as that of clutter collected from the side-looking mode. This means all surface stationary targets in the mainlobe direction also have zero Doppler after the compensation. As a demonstration, the Doppler of the data whose original Doppler spectra are shown in Figure 10 is compensated using (14) and the resultant Doppler spectra are shown in Figure 11. It can be seen that after the Doppler compensation the data appear as if they were collected from the side-looking geometry.

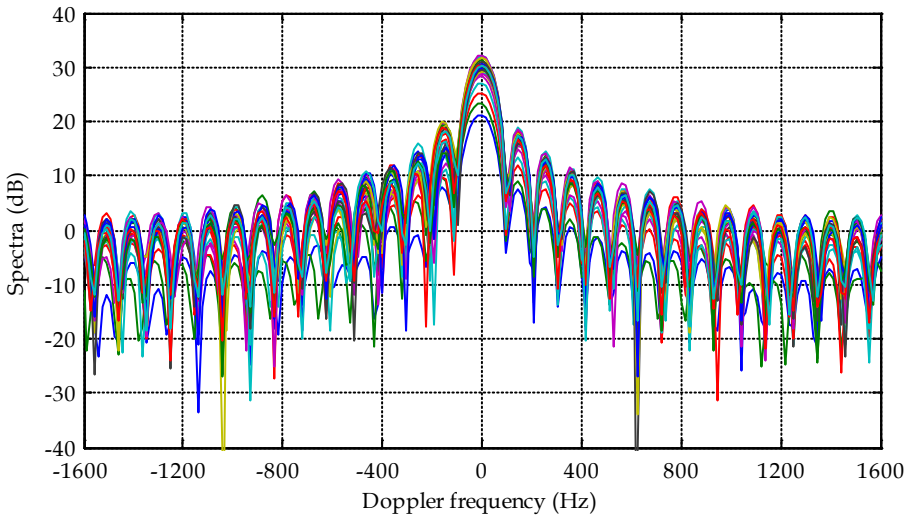

Figure 11: Doppler frequency of the mainlobe clutter shown in Figure 10 is shifted to zero after the Doppler compensation.

Therefore, for a non-side-looking three-dimensional $N \times M \times K$ data cube, where K is the number of range bins, we first perform the Doppler compensation from range bin to range bin. After the Doppler compensation, the data cube can be treated as if it were collected from the side-looking mode, then the remaining detection processing is no different from the processing of the side-looking data, and any of the fully-adaptive or partially-adaptive STAP algorithms can be applied. The comparison between the processing of side-looking data and non-side-looking data is shown in Figure 12.

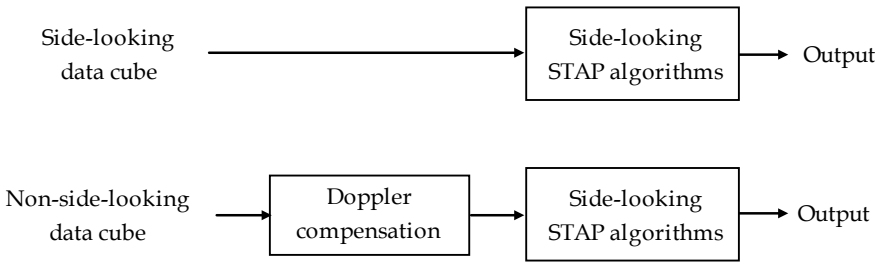

Figure 12: Non-side-looking data cube will be treated as side-looking data cube in STAP after Doppler compensation.

The amount of Doppler compensation given in (14) is for the forward-looking case (0^o from nose). A more general form of (14) is,

$$\Delta f = -\frac{2v_a}{\lambda}\sqrt{1-(h/r)^2}\cos\phi_0 \qquad (15)$$

where ϕ_0 is the azimuth angle the array steers away from the nose ($-180^o \le \phi_0 \le 180^o$). The case of $\phi_0 = \pm 90^o$ is the side-looking case where no Doppler compensation is needed.

Since all parameters of (15) are known *a priori* for the data to be processed, the compensation using (15) should lead to satisfactory results. The effect of crabbing angle is not considered in this compensation scheme and may be treated / compensated separately if necessary. Kreyenkamp and Klemm (2001) argued that parameters of (15) may not be known precisely and there may be a presence of crabbing angle. They proposed a least squares method to estimate the Doppler to be compensated. Unfortunately, the proposed method did not use any radar data, so the estimate was certainly not a least squares estimate. It merely used a Taylor series expansion approximation to replace a precise expression.

3. A Numerical Example

A data cube of sea clutter received by a linear array operated in the forward-looking mode is simulated by GPARM (stands for Generic Phased Array Radar Model) developed by DSTO (Berry *et al.* to be published). Assumptions used in the simulation include,

- Phased array is perfectly calibrated and all radar and platform parameters are known (see Table 1);
- NECAPS model for sea clutter simulation (Branson 2000; Branson *et al.* 2011);
- Range-ambiguous returns are included;
- Propagation effects are include (Coleman and Berry 2013; Coleman *et al.* 2009);
- Receive thermal noise is include;
- Tapering windows to lower sidelobes on receive are used and no tapering window applied to transmit.

The size of the generated data cube is $N \times M \times K$, where $K = 2433$ with a range sampling interval of 15 m (the range resolution is 30 m), the first range bin corresponds to a range-to-height ratio of 2.0 and the last bin to a ratio of 9.3.

The pulse-based spatial spectra as well as the channel-based Doppler spectra shown in Figure 13 and Figure 14 are for a near range bin corresponding to a range-to-height ratio of 2.0. In contrast, the spatial spectra as well as the Doppler spectra shown in Figure 15 and Figure 16 are for a far range bin corresponding to a ratio of 9.3. It can be seen that these spectra are very similar to those shown in Figure 8 to Figure 11, although the simulation used in this section is more sophisticated and many mechanisms such as range-ambiguous returns, propagation effects and a more realistic clutter model are included.

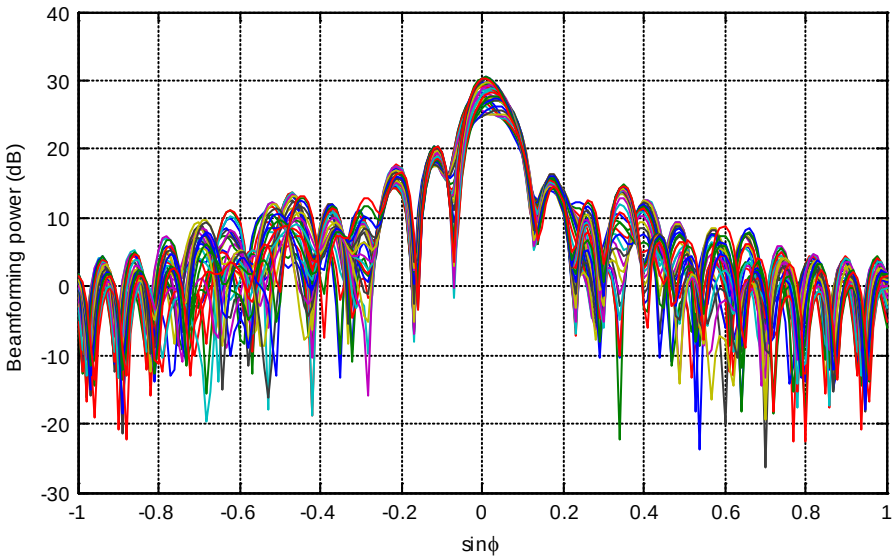

Figure 13: Pulse-based M spatial clutter spectra beamformed from the simulated clutter data for a radar operating in the forward-looking mode with $r/h = 2.0$ *(simulated by GPARM).*

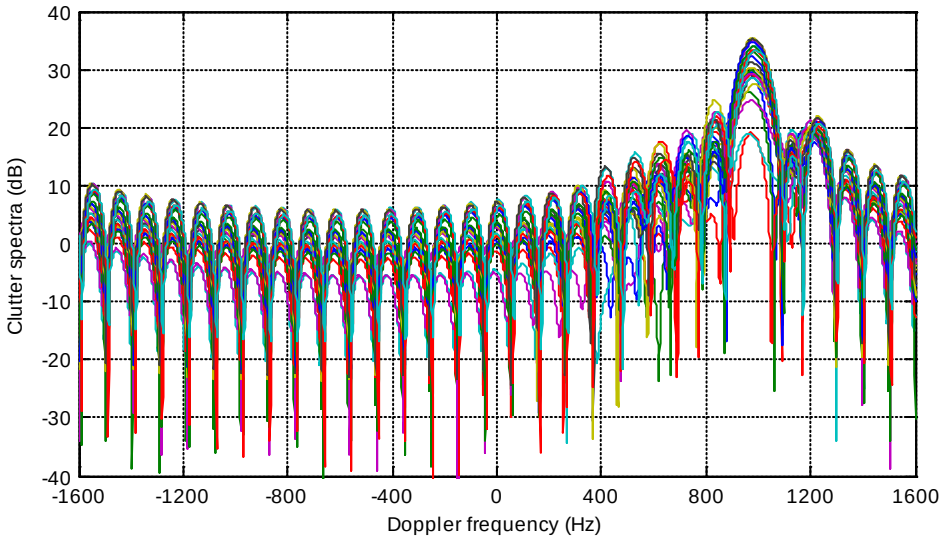

Figure 14: Channel-based N Doppler spectra of the simulated clutter data for a radar operating in the forward-looking mode with $r/h = 2.0$ *(Simulated by GPARM).*

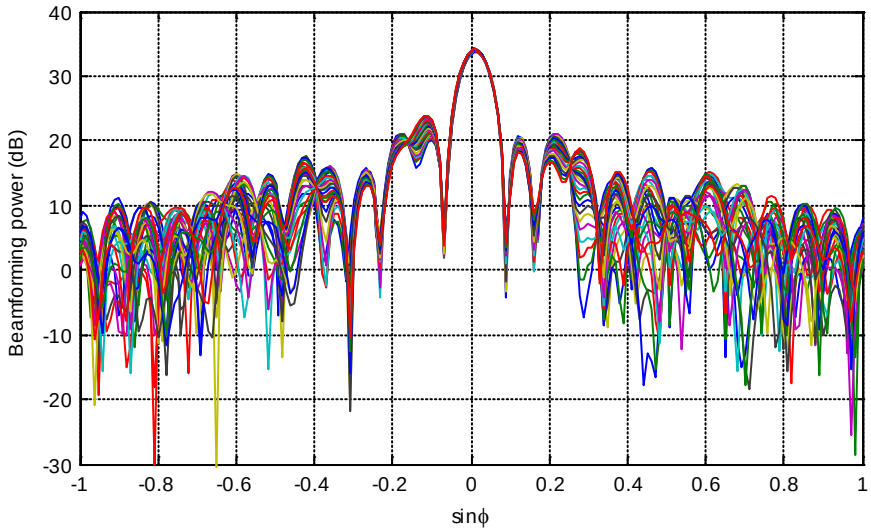

Figure 15: Pulse-based M spatial clutter spectra beamformed from the simulated clutter data for a radar operating in the forward-looking mode with $r/h = 9.3$ *(Simulated by GPARM).*

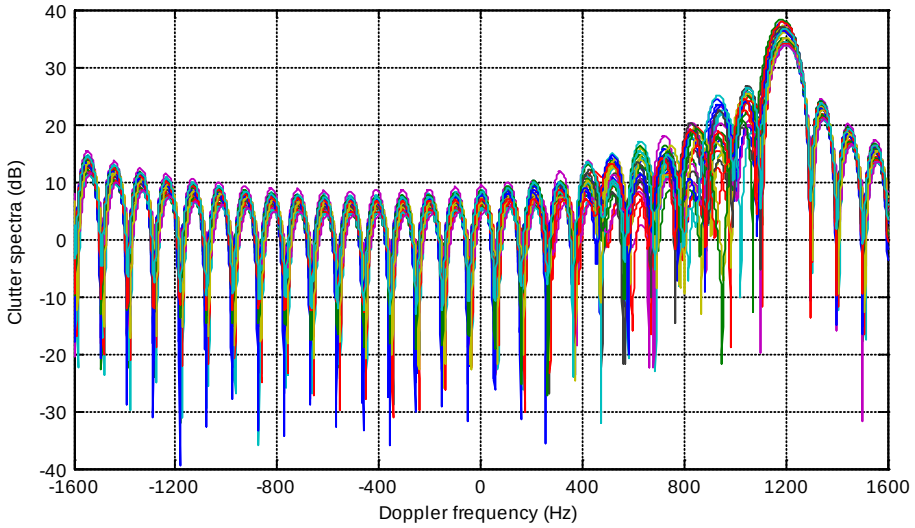

Figure 16: Channel-based N Doppler spectra of the simulated clutter data for a radar operating the in forward-looking mode with $r/h = 9.3$ (Simulated by GPARM).

To investigate the improvement of the Doppler compensation to the detection performance, the signal-to-interference-and-noise ratio improvement factor (SINR IF) is calculated for the case of forward-looking mode, using the data without the Doppler compensation as well as the data after the Doppler compensation.

The covariance matrix of clutter is estimated using the data cube by

$$\hat{\mathbf{R}} = \frac{1}{K}\sum_{k=1}^{K}\boldsymbol{\chi}_k\boldsymbol{\chi}_k^H \qquad (16)$$

The optimal weighting vector is (Ward 1994),

$$\mathbf{w}_{opt} = \hat{\mathbf{R}}^{-1}\mathbf{s} \qquad (17)$$

where $\mathbf{s} = \mathbf{s}_t \otimes \mathbf{s}_s$ is the space-time steering vector; $\mathbf{s}_t$ and $\mathbf{s}_s$ are the temporal and spatial steering vectors, respectively, and given by,

$$\mathbf{s}_t = \left[1 \quad \exp(j2\pi f_t T_r) \quad \cdots \quad \exp(j2\pi f_t T_r (M-1)\right]^T \qquad -f_{PRF}/2 \le f_t \le f_{PRF}/2 \qquad (18)$$

$$\mathbf{s}_s = \mathbf{1}_{N\times 1} \qquad \text{for looking in the mainlobe direction} \qquad (19)$$

The SINR of the optimal processor (17) is given by (Ward 1994),

$$SINR_{out} = \frac{\sigma^2 \xi_t \left| \mathbf{w}_{opt}^H \mathbf{s} \right|^2}{\mathbf{w}_{opt}^H \hat{\mathbf{R}} \mathbf{w}_{opt}^H} \qquad (20)$$

where ξ_t is the single-element single-pulse SNR of the target (i.e., the input target signal-to-noise ratio, $SNR_{in} = \sigma^2 \xi_t / \sigma^2 = \xi_t$).

The SINR IF of a processor is defined as the ratio of output SINR to input SNR. For the above optimal processor, the SINR improvement factor is,

$$SINR_{IF} = \frac{\sigma^2 \left| \mathbf{w}_{opt}^H \mathbf{s} \right|^2}{\mathbf{w}_{opt}^H \hat{\mathbf{R}} \mathbf{w}_{opt}^H} \qquad (21)$$

The SINR IF over the whole Doppler space is calculated using the above simulated clutter data cube. For comparison, Figure 17 shows two curves of SINR IF, one obtained by directly using the data cube to form the covariance matrix (i.e. without the Doppler compensation), the other involving the Doppler compensation. The locations of the two mainlobe clutter notches are different, because the one with the Doppler compensation has made a deliberate Doppler shift so that the mainlobe clutter has a zero Doppler. It can be seen that both curves reach the maximum SINR IF of $10\log_{10}(NM)$ for frequencies differing from that of the mainlobe clutter. The important difference is the width and the depth of the notch. For the dataset that undergoes the Doppler compensation, the notch is narrower and deeper providing better peak cancellation whilst limiting cancellation in the adjacent frequencies. This is because that the mainlobe clutter all has a zero Doppler irrespective of range bins, so data samples can be considered as i.i.d., and the resulting optimal weighting vectors can sufficiently notch the mainlobe clutter while maintaining the minimal detection loss in the vicinities of mainlobe Doppler. On the other hand, the data without the Doppler compensation has varying Doppler for mainlobe clutter, and range data are not i.i.d. As a consequence, the resulting weighting vectors are compromised to be the best for the overall dataset, but not the optimal from range bin to range bin. Hence for near range bins, detection loss occurs in the higher Doppler region whereas the detection loss happens in the lower Doppler region for far range bins. Therefore, the notch for the data without the Doppler compensation is wider. In addition, the depth of the notch is not as deep as it should be, and excessive false-alarms will occur as the processor cannot sufficiently suppress the mainlobe clutter. Note that even after the Doppler compensation the notch is still relatively wide; this is because, according to the simulation, it is a case of sea clutter that itself has a Doppler spectrum centred at zero Hertz (i.e. there is internal clutter motion that spreads the spectrum of the clutter).

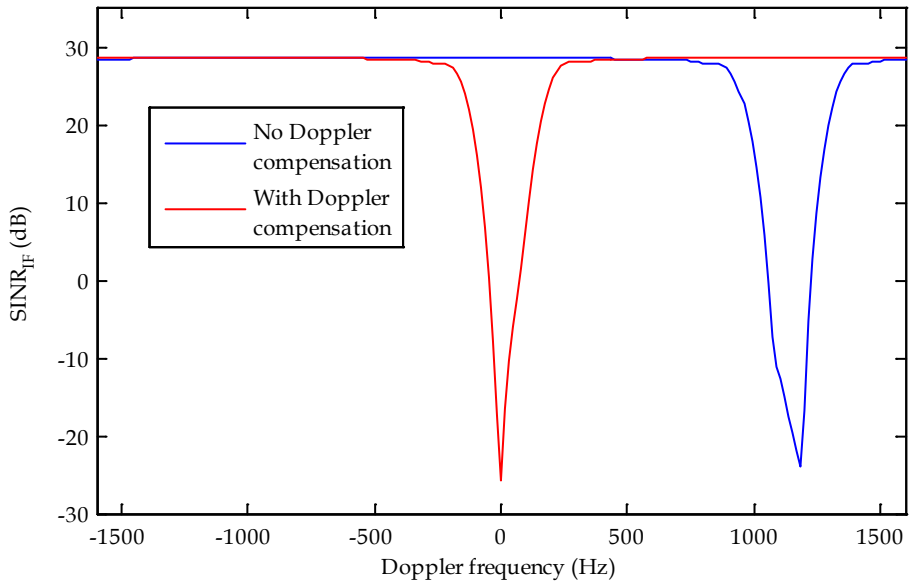

Figure 17: SINR improvement factors with and without Doppler compensation (for the GPARM simulated dataset).

The smaller the range to height ratio, the more severe the problem, if forward-looking data are directly processed using STAP algorithms without the Doppler compensation. The problem, however, will mitigate for higher ratios of range to height. According to Figure 3, once the ratio approaches 10 or higher, the mainlobe clutter Doppler can be considered to be the same for all range bins. In such a scenario the Doppler compensation in the STAP may be omitted.

Although only a generic AEW scenario in a homogenous clutter environment has been assumed in the above simulation, the described Doppler compensation remains the same for heterogeneous clutter environments. Once the data have been compensated, the data can be considered to be collected from the side-looking geometry.

4. Range Ambiguous Clutter and Its Suppression

For airborne radar operating in medium to high PRF modes, range ambiguity is unavoidable. Therefore there is a need to address this issue. The ambiguous range is given by,

$$r_{a(k)} = r + k\frac{cT_r}{2} \qquad k = 1,2,\cdots \tag{22}$$

where c is the speed of light and k denotes the k^{th} ambiguous range, r is the unambiguous range, and $T_r = 1/f_{PRF}$ is the PRI. According to (4), if the constant backscattering coefficient σ_0 clutter model is assumed, the clutter intensity is inversely proportional to the range cubed (since the clutter patch area is proportional to range). Alternatively, if the constant gamma γ_0 clutter model is assumed, because $\sigma_0 = \gamma_0 \sin\theta = \gamma_0 H / r$, where H is the platform height, and θ is the grazing angle (the grazing angle is approximately equal to the depression angle), the clutter intensity will be inversely proportional to the range to the 4^{th} power. As a result, the propagation attenuation of the k^{th} ambiguous range clutter, normalised by the unambiguous range clutter, is,

$$\Delta_k = L_c \log_{10}\left(\frac{r_{a(k)}}{r}\right) = L_c \log_{10}\left(1 + k\frac{cT_r}{2r}\right) \qquad k = 1,2,\cdots \qquad (23)$$

where

$$L_c = \begin{cases} 30 & \text{constant sigma } \sigma_0 \text{ clutter model} \\ 40 & \text{constant gamma } \gamma_0 \text{ clutter model} \end{cases}$$

Since the unambiguous range r is bounded by $0 < r < r_{\max} = cT_r/2$, the propagation attenuation Δ_k is a function of unambiguous range r. Choosing different values of r, we can calculate values of propagation attenuation of the k^{th} ambiguous range clutter which are given in Table 2.

Values given in Table 2, assuming clutter intensity attenuation in a fashion of $(r_{a(k)}/r)^3$ or $(r_{a(k)}/r)^4$ may be conservative for small grazing angles. According to experimental measurements, because of the multipath propagation effect, radar cross-section (RCS) of a point target generally attenuates from $(r_{a(k)}/r)^4$ to $(r_{a(k)}/r)^8$, so that the clutter intensity attenuation can vary from $(r_{a(k)}/r)^3$ to $(r_{a(k)}/r)^7$ for the constant sigma clutter model or from $(r_{a(k)}/r)^4$ to $(r_{a(k)}/r)^8$ for the constant gamma clutter model (Long 2001, Chapter 4).

Table 2: Propagation attenuation of k^{th} ambiguous range clutter (dB), assuming clutter intensity inversely proportional to the range cubed / the range to the 4^{th} power).

Ambiguous range	$r = r_{\max}/10$	$r = r_{\max}/2$	$r = r_{\max}$
$k = 1$	31.2/41.7	14.3/19.1	9.0/12.0
$k = 2$	39.7/52.9	21.0/28.0	14.3/19.1
$k = 3$	44.7/59.7	25.4/33.8	18.1/24.1
$k = 4$	48.4/64.5	28.6/38.2	21.0/28.0

The above discussions assume all range-unambiguous and range-ambiguous clutter to fall in the mainlobe (or in the same sidelobe). In fact, situations can be more complex if range-unambiguous clutter and range-ambiguous clutter fall in different beam lobes. For instance, as depicted in Figure 18, the range-unambiguous clutter falls in the sidelobe whereas the range-ambiguous clutter falls in the mainlobe or vice versa. It is possible that the range-ambiguous clutter can be stronger than the range-unambiguous clutter when radar is operated in high PRF modes.

Since Doppler shifts of non-side-looking clutter are range dependent, and the Doppler compensation scheme discussed earlier only compensates the Doppler shifts of the range-unambiguous clutter. Hence, once the range-ambiguous clutter is involved, the suppression of range-ambiguous clutter becomes more crucial for radar operated in the non-side-looking mode.

4.1 Low Ratio of Range to Height

In general the SINR IF curve may have two or more notches when range-ambiguous clutter is involved. Taking two notches as an example, the second often smaller notch corresponds to the weaker 1st range-ambiguous clutter, and may locate at a different Doppler depending on the radar's looking direction. For a radar operating in the side-looking geometry, the Doppler is range invariant, so the second notch falls in the first and there will be only one notch. For a radar operating in non-side-looking geometries, Doppler is range dependent, so the Doppler frequencies of range-unambiguous mainlobe clutter and range-ambiguous mainlobe clutter are different, resulting in two or more notches. If a radar looks at near range with a low ratio of range to height, the depression angles of the ambiguous range and unambiguous range are very different, and one may use a common beamforming technique in the elevation to null the illumination of the range-ambiguous surface for suppression of range-ambiguous clutter. This requires that the transmit antenna has to be a two-dimensional planar antenna so nulls can be placed in the required elevation beam pattern.

For instance, for the previous numerical example, suppose radar's mainlobe is steered down at $r = 10\,\text{km}$ with $h = 5\,\text{km}$ and $r/h = 2$. According to the given parameters, its first unambiguous range is $r_{a(1)} = 56.875\,\text{km}$. The difference of their depression angles is 25.0^{o} which means that the range-ambiguous clutter will have to enter through an elevation angle of 25.0^{o}. Since their elevation angles are very different, one may utilise a beamforming technique to null the range-ambiguous clutter to remove the second notch from the SINR IF curve, if the array is a 2D planar array. However, this may be hard to do in practice, as there are quite a few parameters determining the ambiguous range and the elevation angle corresponding to range-ambiguous clutter. Some radar systems may have limited degrees of freedom in elevation for beamforming.

4.2 High Ratio of Range to Height

If a radar steers at far range with a high ratio of range to height, the difference of depression angles of unambiguous range and ambiguous range is small, and it is perhaps difficult to null the range-ambiguous clutter using the beamforming technique. However, at a high ratio of range to height, the Doppler of the clutter becomes approximately independent of range, and the range-ambiguous clutter has the same Doppler as that of the range-unambiguous clutter, similar to the side-looking case. Hence the detection loss caused by the range-ambiguous clutter is negligible. The only difference is that the involvement of the ambiguous clutter increases the rank of the clutter covariance matrix, so it requires more sample data to estimate the covariance matrix in order to achieve the desired performance.

4.3 Medium Ratio of Range to Height

It is difficult to null the range-ambiguous clutter when a radar is operated at a medium ratio of range to height, as the difference in depression angles is small. However, the difference of the corresponding Doppler frequencies is also small. Overall the involvement of ambiguous clutter slightly broadens the clutter notch, causing some minor detection loss in the vicinities of the Doppler of mainlobe clutter, which we may have to bear with unless other techniques, such as suppression of range-ambiguous clutter, are further used.

5. Potential Techniques for Suppression of Range-Ambiguous Clutter

5.1 3D Data Processing

Commonly STAP algorithms perform two-dimensional space-time adaptive processing. The space involved normally refers to the azimuth direction. In fact, airborne phased arrays are typically of a rectangular latticed structure. Data from antenna elements in elevation, if available, provide another dimension of processing leading to the so-called 3D STAP. Adding elevation processing under some conditions can offer significant clutter suppression improvement, allowing further suppression of the interference sources that have identical azimuth and Doppler but different elevation from the target signals (Fertig and Krich 2005; Dong 2011).

The achievement of further clutter suppression by adding elevation processing is twofold. First, for close range bins, airborne targets and the ground clutter may have significant elevation angles as shown in Figure 18. Adaptive beamforming processing in elevation can thus separate target signals from undesired interferences, proving clutter suppression in the elevation domain. Secondly, when radar is operated in medium to high PRF modes, the range is often ambiguous as mentioned earlier. In some cases as discussed previously, nothing can be done to mitigate the effect of the range-ambiguous clutter. However, since the range-ambiguous clutter comes from a different elevation angle, a proper adaptive

processing in the elevation domain can filter out the ambiguous range clutter to improve SINR in Doppler regions that are otherwise degraded by the range-ambiguous clutter. In their paper, Fertig and Krich (2005) show an example in which the range-ambiguous clutter is suppressed and target detection improved by 3D STAP.

In principle, 2D STAP algorithms can be readily extended to 3D without any difficulty (Fertig and Krich 2005). The only problem is that adding another dimension in STAP significantly increases the scale of data recording and processing, and enlarges the size of the covariance matrix. Hence the requirements for sample data support and computational budget also significantly increase accordingly.

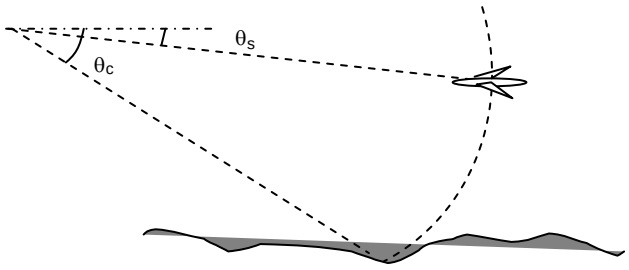

Figure 18: Elevation angles of an airborne target and the ground clutter can be significantly different for close range targets.

5.2 Frequency Diversity Technique

The aforementioned 3D STAP (adaptive in azimuth, elevation and Doppler) greatly increases the computational cost and demands much more sample data to support. In practice, there may not be sufficient i.i.d. samples for estimating the covariance matrix[2]. Recently a concept for using frequency diversity to mitigate/suppress range-angle dependent clutter has been proposed (Baizert *et al.* 2006; Antonik *et al.* 2006b; Sammartino *et al.* 2013). Frequency diverse array (FDA) differs from its conventional phased array counterpart by employing a small frequency increment across array elements. It can generate a range, angle and time dependent beam pattern (Antonik *et al.* 2006b; Huang *et al.* 2008; Wang 2013). The small frequency increment provides additional degrees of freedom (DoF), which lead to a separation of range-ambiguous clutter from range-unambiguous clutter.

[2] It is possible to use previous CPI data for estimating the covariance matrix for the current CPI to overcome the sample data issue (see Dong, Y. (2005), "Approximate invariance of the inverse of the covariance matrix and the resultant pre-built STAP processor", DSTO-RR-0291).

Using FDA to suppress the range-ambiguous clutter is explained in the following. For a FDA the waveform radiated from an array element differs from the others by a carrier frequency increment Δf (Antonik *et al.* 2006a). For a linear array,

$$f_n = f_0 + n\Delta f \qquad n = 0, \cdots, N-1 \tag{24}$$

Assume all N waveforms are mutually orthogonal (de Wit *et al.* 2011), and hence the received signals can be separated in frequency. In order to re-achieve the transmit gain, the received signal is synthesised prior to further processing. In other words, transmit is realised on an element basis whilst receive is achieved using the whole aperture. Signals of different frequencies are then separated.

Let us discuss the spatial frequency of FDA. Consider that the geometry between the array and a distant scatterer is defined by range r (referenced to channel 0), azimuth angle ϕ and depression angle θ. The received signal by the full aperture for the waveform transmitted by the nth channel is (common terms are omitted),

$$\gamma_n(\theta,\phi;r) = \exp\left(j\frac{2\pi f_n}{c}(r + nd\cos\theta\sin\phi)\right)\sum_{k=0}^{N-1}\exp\left(j\frac{2\pi f_n}{c}(r + k\,d\cos\theta\sin\phi)\right) \qquad n = 0, \cdots, N-1 \tag{25}$$

where the first term is the phase corresponding the waveform emitted from the nth channel to the scatterer, and the second sum term is the returned waveform synthesised by the whole aperture. The summation gives,

$$\gamma_n(\theta,\phi;r) = \exp\left[j\frac{2\pi f_n}{c}\left(2r + \left(\frac{N-1}{2} + n\right)d\cos\theta\sin\phi\right)\right]\frac{\sin\left(N\pi\frac{f_n}{c}d\cos\theta\sin\phi\right)}{\sin\left(\pi\frac{f_n}{c}d\cos\theta\sin\phi\right)} \qquad n = 0, \cdots, N-1 \tag{26}$$

Suppose the radar steers to $\phi = 0$, the beamforming of N channels gives,

$$\begin{aligned}\Gamma(\theta,0;r) &= \sum_{k=0}^{N-1}\gamma_k(\theta,0;r) = N\sum_{k=0}^{N-1}\exp\left(j\frac{2\pi f_k}{c}2r\right) \\ &= N\exp\left(j\frac{2\pi f_0}{c}2r\right)\exp\left(j\frac{2\pi\Delta f}{c}(N-1)r\right)\frac{\sin\left(N\frac{2\pi\Delta f}{c}r\right)}{\sin\left(\frac{2\pi\Delta f}{c}r\right)}\end{aligned} \tag{27}$$

Obviously, for $\Delta f = 0$, (27) simplifies to $N^2\exp\left(j\frac{2\pi f_0}{c}2r\right)$, an expected result for the conventional phased array, where N^2 is the round trip coherent processing gain (i.e., a

transmit gain of N and receive gain of N), and $\exp\left(j\frac{2\pi f_0}{c}2r\right)$ is the round trip phase delay.

As shown in (27), the beam pattern in range[3] $|\Gamma(\theta,0;r)|$ periodically reaches maximum when $\sin(2\pi r\Delta f/c)=0$. Locations of $|\Gamma(\theta,0;r)|$ peaks are,

$$r=\frac{k\pi c}{2\pi\Delta f}=\frac{kc}{2\Delta f} \qquad k=0,1,\cdots, \tag{28}$$

Accordingly, $|\Gamma(\theta,0;r)|$ periodically reaches maxima at intervals of $\Delta r=c/(2\Delta f)$. Figure 19 shows the beam pattern in range periodically varying with range. Note that the range shown in the figure is range relative to the range of interest (beam patterns in range are discussed in the far field region). For instance, if we are interested in the radar measurement at $r=r_0$, a phase term of $\exp\left(-j\frac{2\pi f_n}{c}2r_0\right)$ should be compensated for $\gamma_n(\theta,\phi;r)$, $n=0,\cdots,N-1$, so that the radar wave will be focused at $r=r_0$, and the associated beam pattern in range will be the same as what is shown in Figure 19, and the relative range 0 refers to $r=r_0$.

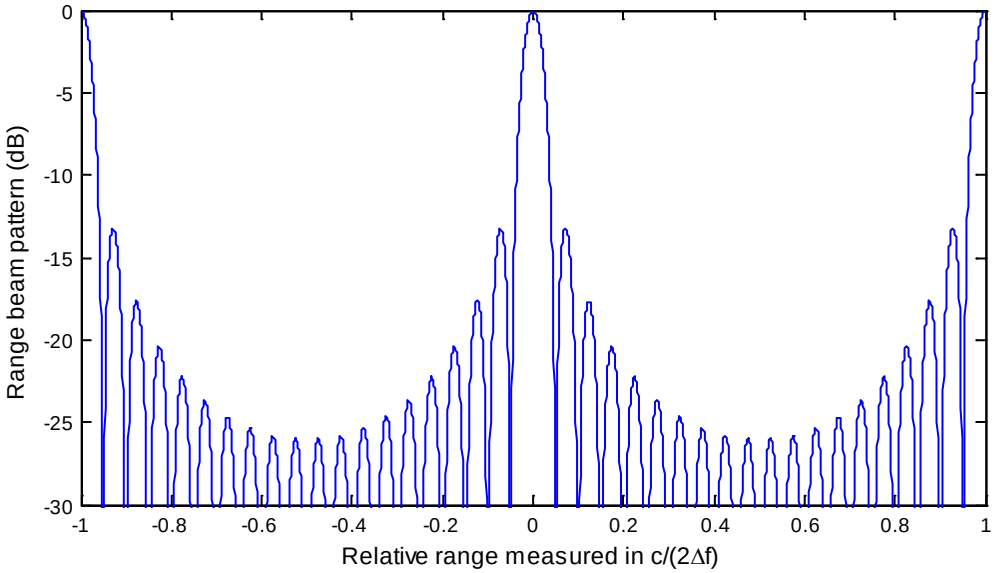

Figure 19: Beam pattern in range ($N=20$).

[3] The beam pattern of traditional radar normally refers to the beam pattern in azimuth as its beam pattern is independent of range. The beam pattern of FDA is however dependent on both azimuth and range. The beam pattern $|\Gamma(\theta,0;r)|$ discussed here is the beam pattern in range, and hence the term "beam pattern in range" is used.

It can be seen that compared to a conventional phased array radar whose beam pattern in range is independent of range, the beam pattern in range of a FDA radar varies periodically in range adding another dimension of DoF. One of its potential applications is the suppression of the range-ambiguous clutter. We recall that the ambiguous range interval is $cT_r/2$ (see (22)). In order to focus at the unambiguous range r, a phaser of $\exp\left(-j\frac{2\pi f_n}{c}2r\right)$ is needed to compensate γ_n, $n=0,\cdots,N-1$. After the compensation, the relative range between the focused range and the first ambiguous range is $cT_r/2$. Because our goal is to suppress the range-ambiguous clutter, we may choose such parameters, so that the first ambiguous range falls in the middle of the two maxima of the beam pattern of Figure 19. This criterion requires,

$$\frac{cT_r}{2}=\frac{c}{2\Delta f}(k_r+1/2) \tag{29}$$

where k_r is a natural number of $k_r=0,1,\cdots$. From (29) one obtains,

$$f_{PRF}=\frac{\Delta f}{k_r+0.5} \tag{30}$$

Accordingly one selects an appropriate integer k_r in such a way so that the resulted f_{PRF} is close to the desired one. With such a selection, the clutter return from the 1st, 3rd, 5th and so on ambiguous range will be suppressed. Alternatively, one may select f_{PRF} by,

$$f_{PRF}=\frac{\Delta f}{k_r+0.25} \tag{31}$$

By this way, the clutter returns from the 1st, 2nd, 3rd and 5th, 6th, 7th ambiguous range and so on will be suppressed. As an example, differences between the selected f_{PRF} and the desired f_{PRF} based on (30) and (31) are given in Table 3.

Table 3: Choose proper PRFs to suppress range-ambiguous clutter ($\Delta f=100$ kHz).

Desired PRF	Selected PRF based on (30)	Selected PRF based on (31)
1000 Hz	995 Hz	998 Hz
2000 Hz	1980 Hz	1990 Hz
3000 Hz	2985 Hz	3008 Hz

In addition to the suppression of range-ambiguous clutter, there is another potential application of FDA. When radar is operated in medium to high PRFs, range becomes ambiguous. In the conventional phased array radar, whether a target presents in

unambiguous range or ambiguous range is not distinguishable, and the radar needs to use different PRFs to discriminate. With the FDA, it requires a unique phase compensation to focus at the range of interest. As a result, if the phase compensation is for the unambiguous range, a target in the ambiguous range will be greatly attenuated or suppressed. To detect a target located in the ambiguous range, the associated phase compensation has to be used. Therefore, there is perhaps no need for DFA to collect different PRF data to determine the true location of target even though the radar is operated in a range-ambiguous PRF.

In the above, the phase compensation is carried out in the radio frequency domain, which may not be convenient. In fact, the phase compensation can be carried out in the baseband. The phase difference between *n*th channel and the reference channel (0th channel) is,

$$\begin{aligned}\Delta\psi_n(\theta,\phi,r) &= \angle\gamma_n(\theta,\phi,r) - \angle\gamma_0(\theta,\phi,r) \\ &= \frac{2\pi n\Delta f}{c}2r + \frac{2\pi}{\lambda_0}\left[1+\frac{\Delta f}{f_0}\left(\frac{N-1}{2}+n\right)\right]n\, d\cos\theta\sin\phi\end{aligned} \tag{32}$$

If there is no frequency diversity, $\Delta f = 0$, the first term vanishes, and the phase difference becomes the familiar one of $\frac{2\pi}{\lambda_0} nd\cos\theta\sin\phi$ for a conventional phased-array radar, which is independent of range. Equation (32) may be written as,

$$\Delta\psi_n = 2\pi f_r + 2\pi f_s \tag{33}$$

Equation (33) shows that with a FDA, the spatial frequency consists of two components: the first one is range dependent, and the second one is orientation dependent. In the processing, a proper phaser of $\exp\left(-j\frac{2\pi n\Delta f}{c}2r\right)$, $n = 0,1,\cdots,N-1$, has to be compensated for the range of interest, so that the waveform focuses at the range of interest, and range-ambiguous clutter is suppressed. The remaining processing will be no different to the conventional phased-array data, rather than using a different spatial steering vector. All STAP algorithms developed for the conventional phased-array can be applied.

There is a need to justify that the Doppler properties of clutter is approximately unaffected. For a clutter patch located at (θ,ϕ), the associated Doppler for the *n*th channel is,

$$f_{an} = \frac{2v_a}{\lambda_n}\cos\theta\sin\phi = \frac{2v_a}{c}f_0(1+n\Delta f/f_0)\cos\theta\sin\phi \approx \frac{2v_a}{\lambda_0}\cos\theta\sin\phi \tag{34}$$

Therefore, the effect of the frequency diversity on the Doppler is negligible.

In summary, a block diagram of the FDA data processing technique to suppress range-ambiguous clutter is depicted in Figure 20. The main differences between the FDA data processing and the conventional phased-array data processing include,

- Array synthesis is performed on receive for FDA, whereas it is automatically performed at transmit for a phased-array;
- Phase compensation is required for FDA data to focus the radar wave at the range of interest whereas no such a step is required for the phased-array data;
- The spatial steering vector is different.

The remaining STAP processing is identical for both FDA and phased-array data.

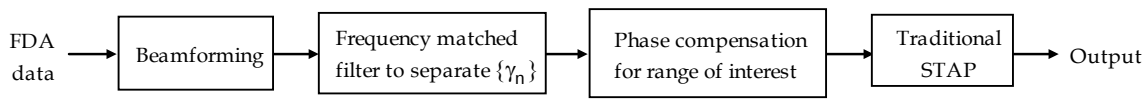

Figure 20: Block diagram of FDA data processing to suppress range-ambiguous clutter.

Detailed architectures, characteristics and techniques of the FDA radar will be investigated in a separate report.

6. Conclusions

This Technical Note is a supplement to an earlier DSTO Technical Note, "Overview of STAP algorithms" (Dong 2011). It is aimed at the processing of phased array data collected from non-side-looking geometries. In general, STAP algorithms developed for a radar operating in the side-looking mode cannot be directly applied to data collected by a radar operating in non-side-looking modes, including the forward-looking mode. A simple Doppler compensation scheme is proposed, so that the Doppler of mainlobe clutter is shifted to zero and becomes range invariant, like the clutter data collected from the side-looking geometry. After the Doppler compensation, all STAP algorithms developed for the side-looking geometry can be applied.

Also briefly discussed are a few potential techniques for the suppression of range-ambiguous clutter, including beamforming techniques and the 3D STAP. The frequency diversity technique discussed in literature is interesting but further study is needed. A detailed study of frequency diverse array will be reported separately in the future.

7. Acknowledgement

The author thanks Mr Gavin Currie and Dr Paul Berry for introducing the GPARM software and assisting in generating the sea clutter data cube simulated by the GPARM.

Drs Andrew Shaw and Paul Berry's technical and grammatical comments on the manuscript are also greatly acknowledged.

References

Antonik, P., Wicks, M. C., Griffiths, H. D., and Backer, C. J. (2006a), "Frequency diverse array radars", *Proceedings of IEEE Radar Conference*, Verona, NY**:** 215-217.

Antonik, P., Wicks, M. C., Griffiths, H. D., and Backer, C. J. (2006b), "Range-dependent beamforming using element level waveform diversity", *Proceedings of International Waveform Diversity and Design Conference***:** 140-144.

Baizert, P., Hale, T. B., Temple, M. A., and Wicks, M. C. (2006), "Forward-looking radar GMTI benefits using a linear frequency diverse array", *Electronics Letters*, **42**(22), 1311-1312.

Berry, P. E., Currie, G., and Summers, A. (to be published), "Phased-array radar simulation model specification", DSTO-TR-xxxx, Defence Science and Technology Organisation, Australia.

Branson, J. (2000), "Naval Environmental clutter, attennuation and propagation - NECAPS 3", *DERA*.

Branson, J., Billett, S., Neil, H., and Will, W. (2011), "Naval environmental clutter, attennuation and propagation specification - NECAPS 4.1", QinetiQ/D&TS/SEA/TS0700336/2.1, QinetiQ.

Coleman, C., and Berry, P. E. (2013), "A Kirchhoff integral approach to radar propagation over a rough sea", *Proceedings of IEEE International Conference on radar*.

Coleman, C., Yardley, H., and Berry, P. E. (2009), "GRADAR: A radar propagation modelling tool for frequencies from VHF to microwave", *Proceedings of International Radar Conference*.

de Wit, J. J. M., van Rossum, W. L., and de Jong, A. J. (2011), "Orthogonal waveforms for FMCW MIMO radar", *Proceedings of IEEE Radar Conference*, Kansas, MO**:** 686-691.

Dong, Y. (2011), "Overview of STAP algorithms", Technical Note, DSTO-TN-0992, Defence Science and Technology Organisation, Australia.

Fertig, L. B., and Krich, S. I. (2005), "Benefits of 3D-STAP for X-band GMTI airborne radars", *Adaptive Sensor Array Processing (ASAP) Workshop*, MIT, MA.

Guerci, J. R. (2003), *Space-Time Adaptive Processing for Radar*, Boston, Artech House.

Guerci, J. R. (2010), *Cognitive Radar*, Norwood, MA, Artech House Inc.

Himed, B., Wang, P., and Li, H. (2013), "Tutorial: STAP techniques and applications ", *IEEE International Conference on Radar*, Adelaide.

Huang, J. J., Tong, K. F., and Backer, C. J. (2008), "Frequency diverse array with beam scanning feature", *Proceedings of IEEE Antennas and Propagation Society International Symposium* San Diago, California**:** 1-4.

Klemm, R. K. (2002), *Principles of Space-Time Adaptive Processing*, 2nd, London, IEE.

Klemm, R. K., editor, (2004), *Applications of Space-Time Adaptive Processing*, London, IEE.

Kreyenkamp, O., and Klemm, R. (2001), "Doppler compensation in forward-looking STAP radar", *IEE Proc.~Radar, Sonar Navig.*, **148**(5), 253-258.

Lapierre, F. D., Ries, P., and Verly, J. G. (2009), "Foundation for mitigating range dependence in radar space-time adaptive processing ", *IET Radar, Sonar and Navig.*, **3**(1), 18-29.

Long, M. W. (2001), *Radar Reflectivity of Land and Sea*, 3rd Ed, Dedham, MA, Artech House.

Melvin, W. L. (2004), "A STAP overview", *IEEE A&E Systems Magazine*, **19**(1), 19-35.

Sammartino, P. F., Backer, C. J., and Griffiths, H. D. (2013), "Frequency diverse MIMO techniques for radar", *IEEE Trans on Aerospace and Electronic Systems*, **49**(1), 201-222.

Wang, W. Q. (2013), "Range-angle dependent trasmit beampattern synthesis for linear frequency diverse arrays", *IEEE Trans on Antennas and Propagation*, **61**(8), 4073-4081.

Wang, Y. L., Peng, Y. N., and Bao, Z. (1997), "Space-time adaptive processing for airborne radar with various array orientations", *IEE Proc.~Radar, Sonar Navig.*, **144**(6), 330-340.

Ward, J. (1994), "Space-time adaptive processing for airborne radar", Technical Report, 1015, Lincoln Laboratory, MIT.

DEFENCE SCIENCE AND TECHNOLOGY GROUP DOCUMENT CONTROL DATA	1. DLM/CAVEAT (OF DOCUMENT)

2. TITLE	3. SECURITY CLASSIFICATION (FOR UNCLASSIFIED REPORTS THAT ARE LIMITED RELEASE USE (L) NEXT TO DOCUMENT CLASSIFICATION)
Doppler Compensation for Airborne Non-Side-Looking Phased-Array Radar	Document (U) Title (U) Abstract (U)
4. AUTHOR(S) Yunhan Dong	5. CORPORATE AUTHOR Defence Science and Technology Group PO Box 1500 Edinburgh South Australia 5111 Australia

6a. DST Group NUMBER	6b. AR NUMBER	6c. TYPE OF REPORT	7. DOCUMENT DATE
DST-Group-TN-1461	AR-016-420	Technical Report	September 2015

8. FILE NUMBER	9. TASK NUMBER	10. TASK SPONSOR	11. NO. OF PAGES	12. NO. OF REFERENCES
			28	25

13. DST Group Publications Repository	14. RELEASE AUTHORITY
http://dspace.dsto.defence.gov.au/dspace/	Chief, National Security and ISR Division

15. SECONDARY RELEASE STATEMENT OF THIS DOCUMENT

Approved for public release

OVERSEAS ENQUIRIES OUTSIDE STATED LIMITATIONS SHOULD BE REFERRED THROUGH DOCUMENT EXCHANGE, PO BOX 1500, EDINBURGH, SA 5111

16. DELIBERATE ANNOUNCEMENT

No Limitations

17. CITATION IN OTHER DOCUMENTS Yes

18. RESEARCH LIBRARY THESAURUS

Space-time adaptive processing, Airborne phased-array radar, Non-side-looking, Doppler compensation

19. ABSTRACT

As a supplement to an earlier DSTO Technical Note, "Overview of STAP algorithms", this Technical Note examines processing of phased array data collected from non-side-looking geometries. Space-time adaptive processing (STAP) algorithms developed for the radar operating in the side-looking mode cannot in general be directly applied to radar operating in non-side-looking modes, including the forward-looking mode. A simple Doppler compensation scheme is described, so that the Doppler frequency of mainlobe clutter is shifted to zero and becomes range invariant, like the clutter data collected from the side-looking geometry. After Doppler compensation, all STAP algorithms developed for the side-looking geometry can be applied. Also briefly discussed are some techniques for suppression of range-ambiguous clutter, including so-called 3D STAP and frequency diversity technology.